A Prospective Comparison of [^{18}F]FAPI-42 and [^{68}Ga]Ga-FAPI-04 PET/CT in Patients With Various Cancers

Kongzhen Hu
Southern Medical University Nanfang Hospital
Lijuan Wang
Southern Medical University Nanfang Hospital
Hubing Wu
Southern Medical University Nanfang Hospital
Shun Huang
Southern Medical University Nanfang Hospital
Ying Tian
Southern Medical University Nanfang Hospital
Qiaoyu Wang
Southern Medical University Nanfang Hospital
Caixia Xiao
Southern Medical University Nanfang Hospital
Yanjiang Han
Southern Medical University Nanfang Hospital
Ganghua Tang (gtang0224@smu.edu.cn)
Southern Medical University Nanfang Hospital https://orcid.org/0000-0001-6288-5578

Research Article

Keywords: Fibroblast activation protein, [18F]FAPI-42, [68Ga]Ga-FAPI-04, PET/CT

Posted Date: September 8th, 2021

DOI: https://doi.org/10.21203/rs.3.rs-873563/v1

Abstract

Purpose: [18F]FAPI-42 is a new fibroblast activation protein (FAP) specific tracer used for cancer imaging. Here, we describe the *in vivo* evaluation of [18F]FAPI-42 and compared intra-individual biodistribution, tumor uptake, and detection ability to [68Ga]Ga-FAPI-04.

Methods: A total of 22 patients with various types of cancer received [18F]FAPI-42 whole-body positron emission tomography/computed tomography (PET/CT). Among them, 4 patients underwent PET/CT scans, including an early dynamic 20-min, static 1-hour and static 2-hours. The *in vivo* biodistribution in normal organs and tumor uptake were semi-quantitatively evaluated using the standardized uptake value (SUV) and tumor-to-background ratio (TBR). Furthermore, both [18F]FAPI-42 and [68Ga]Ga-FAPI-04 PET/CT were performed in 12 patients to compare biodistribution, tumor uptake, and tumor detection ability.

Results: [18F]FAPI-42 uptake in the tumors was rapid and reached a high level with an average SUVmax of 15.8 at 18 minutes, which stayed at a similarly high level to 2 hours. The optimal image acquisition time for [18F]FAPI-42 was determined to be 1 hour post injection. Compared to [68Ga]Ga-FAPI-04, [18F]FAPI-42 had a higher uptake in the parotid, salivary gland, thyroid, and pancreas ($P < 0.05$). For tumor detection, [18F]FAPI-42 had a high uptake and could be clearly visualized in the lesions. [18F]FAPI-42 and [68Ga]Ga-FAPI-04 showed the same detectability for 144 positive lesions. In addition, [18F]FAPI-42 had a higher SUVmax in liver and bone lesions ($P < 0.05$) and higher TBRs in liver, bone, lymph node, pleura and peritonea lesions (all $P < 0.05$).

Conclusion: The present study demonstrates that [18F]FAPI-42 is a good tracer for imaging malignant tumors and exhibited comparable lesion detectability to [68Ga]Ga-FAPI-04. The 1-hour scan is an appropriate time for tumor detection and is superior to the early 10-min scan for the detection of small lesions.

Trial registration Chinese Clinical Trial Registry (ChiCTR2100045757)

Introduction

Fibroblast activation protein (FAP) is a transmembrane serine protease that is expressed in stromal fibroblasts in more than 90% of epithelial cancers as well as in malignant cells in glioblastoma and pancreatic, breast, colorectal, cervical, and oral squamous cell carcinomas [1, 2]. Overexpression of FAP is associated with high local tumor motility and invasiveness, decreased survival, and poor prognosis in cancer patients [2–4]. It has been shown that FAP is also upregulated in lesions associated with wound healing, atherosclerotic plaques, rheumatoid arthritis, idiopathic pulmonary fibrosis, and hepatic fibrosis [5–9], but is expressed at a negligible or non-detectable level in most normal adult tissues under physiological conditions. Therefore, FAP is considered a good target for diagnosis and treatment of tumors and non-malignant diseases associated with FAP expression. Accordingly, FAP-targeted positron emission tomography/computed tomography (PET/CT) has emerged as a new technique for imaging

cancers. The most common FAP tracer is a quinoline-based FAP-ligand radiolabeled with the generator radionuclide ^{68}Ga ($T_{1/2}$ = 67.7 min, 88.9 % β^+) ([^{68}Ga]Ga-FAPI-04). [^{68}Ga]Ga-FAPI-04 PET/CT has been demonstrated to be a good imaging modality for 28 types of cancer and offers higher tumor to non-tumor (T/NT) contrast and higher tumor detectability compared to [^{18}F]FDG PET/CT [10–18]. However, [^{68}Ga]Ga-FAPI-04 is limited by the relatively short half-life of ^{68}Ga and availability from the ^{68}Ge/^{68}Ga-generator, which allows only one or two elution per day and batch production of approximately 1–3 patient doses per elution. In this context, ^{18}F-labeled FAP tracers may represent a promising alternative for FAP imaging. ^{18}F-flourine, as is well-known, is a positron emitter that is commonly available due to extensively equipped cyclotron worldwide and can be produced in a large amount to meet the requirements of a large number of patients. ^{18}F-labeled radiopharmaceuticals have a longer half-life ($T_{1/2}$ = 109.8 min) and can thus be delivered over longer distances. Furthermore, the low positron energy of ^{18}F ($\leq$ 635 keV) enables a short positron linear range in tissue (2.3 mm), resulting in the highest resolution PET images of all available positron emitters [19].

The ^{18}F-labeled FAP ligand, [^{18}F]FAPI-42, has the same pharmacophore as [^{68}Ga]Ga-FAPI-04 with the exception of the replacement of the chelator DOTA by NOTA. This tracer has only been recently clinically introduced [20, 21] and has not yet been bench-marked against other FAP tracers. Wang et al. reported that [^{18}F]FAPI-42 had a good performance for depicting malignant tumors [20]. However, it is not precisely clear whether [^{18}F]FAPI-42 performs as well as [^{68}Ga]Ga-FAPI-04 in the detection of tumors. Furthermore, it is also necessary to determine the optimal time for image acquisition. Thus, we performed a prospective study to compare the tumor detectability of [^{18}F]FAPI-42 with [^{68}Ga]Ga-FAPI-04 and determine the optimal image acquisition time for [^{18}F]FAPI-42.

Materials And Methods

Study design and patient population

This study was approved by the institutional review board of the Ethics Committee of Nanfang Hospital (No. NFEC-2020-205) and registered at Chinese Clinical Trial Registry (ChiCTR2100045757). All patients signed a written informed consent before participation and all procedures were conducted in accordance with the Declaration of Helsinki.

Patients were consecutively recruited for enrollment in this study from April 2021 to July 2021. The inclusion criteria were as follows: (1) patients with newly diagnosed cancer who had not received any previous treatment or patients with recurrent or post-treatment metastatic cancer who had not received any treatment within the last three months; (2) primary malignancies confirmed by pathology; and (3) patients who agreed to undergo the two above-described PET/CT scans. The exclusion criteria were: (1) patients with another primary malignancy at the time of examination; (2) patients who suffered from severe hepatic and renal insufficiency; and (3) patients who refused to undergo the scans.

The primary malignancy was diagnosed by biopsy and histopathological examination. Diagnosis of lymph node metastasis and distant metastasis was established by multiple imaging modalities, including magnetic resonance imaging (MRI) of the brain, chest CT, abdominal ultrasound, whole-body bone scan, and whole-body PET/CT.

Radiopharmaceuticals

The radiolabeling precursors were obtained from Nanchang TanzhenBio Co., Ltd. (Nanchang, China) with high chemical purity (>95%). [^{18}F]FAPI-42 was produced using a fully automated process as previously reported [22]. In brief, [^{18}F]F^- (37–74 GBq) was transferred into the module and trapped on a Sep-Pak Plus QMA (Waters Corporation, preconditioned with 5 mL of 0.5 M sodium acetate buffer pH 3.9 and 10 mL of water) and eluted using 0.35 mL of 0.5 M sodium acetate buffer pH 3.9 to a mixture of $AlCl_3$ (40.0 nmol, 20.0 µL, 2.0 mM in 0.2 M sodium acetate buffer pH 4.0) and precursor NOTA-FAPI-42 (80.0 nmol) in 300 µL dimethyl sulfoxide (DMSO). After heating for 15 min at 105 ºC, the mixture was cooled, diluted with 5 mL of water, and transferred over an activated HLB cartridge (Waters Corporation, preconditioned with 5 mL ethanol and 10 mL water). Next, the HLB cartridge was washed with 20 mL of water, eluted with 1 mL of ethanol/water (1/1, v/v), and flushed using 10 mL of NaCl 0.9%. The eluate was then passed through a sterile Millipore filter (0.22 µm) into a sterile vial.

[^{68}Ga]Ga-FAPI-04 was manually synthesized as previously described [10,12,23]. Briefly, $^{68}GaCl_3$ was achieved by adding 4.00 mL ^{68}Ge/^{68}Ga-generator eluate (0.05 M hydrochloric acid; 0.74-1.48 GBq) to a solution of DOTA-FAPI-04 (25 nmol) in 0.25 mol/L NaOAc aqueous (1 mL). The reaction mixture was heated at 100 ºC for 10 min and purified by simple solid-phase extraction of the product by cartridge separation. Analysis and quality control of the prepared products were performed as previously reported [11,12,20].

Imaging procedures

All patients underwent both [^{18}F]FAPI-42 and [^{68}Ga]Ga-FAPI-04 PET/CT scans on two consecutive days. PET/CT imaging was performed using a total-body PET/CT scanner (uEXPLORER, United Imaging Healthcare; Shanghai, China). For each patient, both examinations were performed on the same scanner.

Before FAPI administration, patients were instructed to fast for at least 2 hours in order to reduce hepatobiliary excretion. The PET/CT scan was performed approximately at 1 hour after intravenous injection of [^{18}F]FAPI-42/[^{68}Ga]Ga-FAPI-04 (1.85–3.7 MBq/kg, 0.05–0.1 mCi/kg). The PET scan was performed with a 5-min single bed position 3D acquisition. Low-dose CT (80 mA, 120 kVp) was acquired for attenuation correction and all corrections applied to the reconstructed images, and for anatomic localization of lesions. All data were reconstructed using list-mode OSEM-PSF-TOF [24,25].

All patients underwent [^{18}F]FAPI-42 PET/CT scanning. Among them, 4 patients' PET-scans were acquired at an early 20-min dynamic scan, 1-hour and 2-hours after administration of [^{18}F]FAPI-42. Twelve patients

also underwent [^{68}Ga]Ga-FAPI-04 PET/CT scanning for comparison.

Imaging interpretation

The acquired CT and PET images were sent to a MedEx workstation for registration, fusion, and measurement. Two experienced nuclear physicians with more than 10 years of certificated experience for each scan independently performed image interpretation and any disagreements were resolved by consensus. Any focal accumulations of [^{18}F]FAPI-42 or [^{68}Ga]Ga-FAPI-04 that was higher than the neighboring tissue was interpreted as a positive lesion. Tumor tracer uptake was quantified by the maximal standardized uptake value (SUVmax) and target-to-background ratio (TBR). The region of interest (ROI) was drawn along the margins of the lesion on the axial PET image and automatically adapted to a three-dimensional volume-of-interest at a 60% isocontour, which was used to measure the SUVmax. TBR was calculated by dividing the SUVmax of the lesion by the SUVmean of the organs (brain background for brain lesions, lung background for lung and pleura lesions, aortic lumen background for lymph nodes, liver background for liver lesions, adrenal glands background for adrenal glands lesions, L5 background for bone lesions, gluteal muscle background for all other lesions). Tumors with a diameter larger than 1 cm were defined as large lesions, while tumors with a diameter smaller than 1 cm were defined as small lesions.

Any drug-related side effects were recorded and the vital parameters of the patients were observed for one week.

Statistical analysis

Normally distributed variables are reported as the means ± standard deviations while skewed variables are reported as the medians (range). The differences in SUVmax and TBR between [^{18}F]FAPI-42 and [^{68}Ga]Ga-FAPI-04 were evaluated using the paired *t*-test (normally distributed variables) or Wilcoxon signed-rank test (skewed variables). Analyses were performed using (SPSS, version 22.0; IBM, Armonk, NY). Two-tailed *P* values less than 0.05 were considered indicative of a statistically significant difference.

Results

Patient characteristics

A total of 22 patients (12 males, 10 females; median age, 55.5 years; range, 23–74 years) with various malignant tumors were prospectively enrolled, including 6 patients with lung cancer, 6 patients with liver cancer, 5 patients with colorectal cancer, and 1 patient each with stomach cancer, esophageal cancer, carcinosarcoma of the cheek, celiac neuroendocrine carcinoma, and clear cell carcinoma of the bladder (Table 1). Among them, 12 patients were newly diagnosed and the other 10 patients had relapse tumors after single or multiple modality treatments. Twelve patients had □ staged diseases, 17 patients had local advanced staged diseases, and 3 patients had early staged diseases (Table 1).

Safety

No drug-related side effects were reported during or after [^{18}F]FAPI-42 or [^{68}Ga]Ga-FAPI-04 PET/CT. PET imaging was well tolerated by all patients. Vital parameters remained stable and no patient reported any new symptoms during the observation period.

Dynamic scans of [^{18}F]FAPI-42

The maximum intensity projection (MIP) and biodistribution data assessed by SUV kinetics for one patient (male) are shown in Fig. 1. The images and SUV kinetics for the other three patients are available in Supplemental Fig. 1-3. The pooled SUVmax and tumor SUVmax/organ SUVmean for all four patients that underwent this scan are summarized in Fig. 2a and 2b. The highest average normal organ SUVmax at all time points was observed in the kidneys, decreasing from an average SUVmax of 238 at 10 min to 27.1 by 2 hours (decline of 89%). Tracer uptake in the tumor was rapid and showed excellent retention with an average SUVmax of 15.8 at 18 min, and 15.3 at 2 hours (decrease of 3%). The SUVmax of the organs decreased in all patients 5 min post-injection (p.i.) to the last time point, while TBRs increased with time (with the exception of the gallbladder TBR). The highest TBR among all timepoints was observed in the lungs, small intestine, and bone, with a ratio of 54.1, 40.3 and 26.9.

The SUVmax and TBR (blood) for large and small lesions are summarized in Fig. 2c and 2d. Although some small lesions could be visualized at the early 10-min scan, other lesions were still indistinct due to low TBR (blood) (2.6 ± 0.64). At the 1-hour scan, although the increase in SUVmax was not significantly different than the 10-min scan (11.3 ± 4.1 *vs.* 7.7 ± 1.5, $P = 0.05$), the TBR (blood) increased significantly to a much higher level (8.1 ± 2.7 vs. 2.6 ± 0.64, $P = 0.0076$) and the small lesions were all clearly visualized (Fig. 1). The TBR further increased from 1 hour to 2 hours; however, this did not result in more lesions detected. For detection of large tumors, the lesions could be clearly visualized at the early 10-min scan, although they were clearer at the 1-hour and 2-hour scans.

Biodistribution comparison between [^{18}F]FAPI-42 and [^{68}Ga]Ga-FAPI-04 PET/CT

In the total 22 patients, [^{18}F]FAPI-42 PET/CT demonstrated intense radioactivity in the urinary tract, indicating that the kidneys were the main excretory organs. Intense uptake of the radioactivity was also observed in the gallbladder and common bile duct, implying that some [^{18}F]FAPI-42 was also eliminated via the hepatobiliary system. Moderate uptake of radioactivity was seen in other organs in some patients, including the submandibular gland (14/22), thyroid (12/22), and pancreas (19/22), similar to the findings of the dynamic scan. Only minimal or mild physiological uptake was observed in other organs and tissue, including the brain, parotid, oral mucosa, lung, myocardium, liver, intestine, fat, spine, and muscle. Radioactivity in bones was low, suggesting that no defluorination occurred *in vivo* (Fig. 3).

Compared with [^{18}F]FAPI-42, [^{68}Ga]Ga-FAPI-04 showed similar uptake of radioactivity in the urinary tract (9.6 ± 7.3 vs. 9.5 ± 7.4, $t = 0.022$, $P = 0.983$), but lower accumulation of radioactivity in the gallbladder and common bile duct (10.5 ± 6.2 vs. 0.9 ± 1.1, $t = 4.461$, $P = 0.001$ and 4.2 ± 2.3 vs.1.1 ± 0.4, $t = 3.753$,

P = 0.003, respectively). Accumulation of [^{68}Ga]Ga-FAPI-04 in the parotid, salivary gland, thyroid, and pancreas was also lower than that of ^{18}F-FAPI-42 (P < 0.05). There were no significant differences in uptake between the two tracers in other organs or tissues (all P > 0.05; Fig. 3).

Comparison of tumor detection and tumor uptake between [^{18}F]FAPI-42 and [^{68}Ga]Ga-FAPI-04 PET/CT

On ^{18}F-FAPI -42 PET/CT images, the uptake of [^{18}F]FAPI-42 in tumors was intense and the lesions could be clearly visualized (Fig. 4). [^{18}F]FAPI-42 PET/CT was positive in all 22 enrolled patients. [^{18}F]FAPI-42 PET/CT depicted primary and relapse tumors in 16 patients, suspected lymph node metastases in 14 patients and suspected distant metastases in 14 patients, including lung lesions in 4 patients, pleural lesions in 5 patients, liver lesions in 6 patients, bone lesions in 4 patients, peritoneal lesions in 2 patients and other suspected metastases in 3 patients. In the 12 patients who received dual-tracer scans, both PET/CT demonstrated the same positive detection for 144 lesions (Table 2). In the visual analysis, [^{18}F]FAPI-42 and [^{68}Ga]Ga-FAPI-04 PET/CT showed comparable results for primary tumors, lymph node lesions, pleural lesions, and peritoneal lesions in terms of both patient-based and lesion-based comparison (Table 2). However, liver and bone lesions were more clearly visualized by [^{18}F]FAPI-42 PET/CT than [^{68}Ga]Ga-FAPI-04 PET/CT (P 0.05; Fig. 5).

No significant differences in SUVmax between [^{18}F]FAPI-42 and [^{68}Ga]Ga-FAPI-04 were found in the primary tumors, lymph node lesions, pleural lesions , or peritoneal lesions (all P > 0.05; Fig. 6). However, uptake of [^{18}F]FAPI-42 was observed to be higher in liver and bone lesions (P 0.05; Fig. 6). Similarly, no significant difference in TBR was found between [^{18}F]FAPI-42 and [^{68}Ga]Ga-FAPI-04 in the primary tumors and lung lesions (P > 0.05). However, the TBR of [^{18}F]FAPI-42 was significantly higher compared to [^{68}Ga]Ga-FAPI-04 not only in liver and bone lesions (P < 0.05), but also in lymph node, pleura, and peritoneum lesions (P < 0.05; Fig.7).

Discussion

^{68}Ga-labeled FAP probes have recently been proven useful for the detection of tumors with high expression of FAP and can be used for imaging various cancers [12, 26–28]. To take advantage of the favorable properties of fluorine-18, a few ^{18}F-labeled FAPI probes have been introduced for PET imaging [20, 21, 27, 29]. However, clinical data comparing ^{68}Ga-labeled and ^{18}F-labeled FAP tracers are scarce and the suitable time for the detection of tumors also needs to be identified for ^{18}F-labeled FAP probes. In the present study, we compared biodistribution and lesion detectability between the FAP tracers [^{18}F]FAPI-42 and [^{68}Ga]Ga-FAPI-04 in cancer patients. In addition, the optimal image acquisition time for [^{18}F]FAPI-42 was established.

The biodistribution of [^{18}F]FAPI-42 in four cancer patients from 0 to 2 hours after tracer administration demonstrated rapid and high tumor uptake and satisfactory retention, while normal organs showed rapid radioactivity decreases and excretion through the kidneys. Combined with the biodistribution results in

another 12 cancer patients, [^{18}F]FAPI-42 demonstrated that the excretion pathway of [^{18}F]FAPI-42 is predominantly from urinary and biliary systems, which is similar to reports for the tracers [^{18}F]FAPI-74, [^{68}Ga]Ga-FAPI-04, and [^{68}Ga]Ga-FAPI-46 [12, 27, 30].

The optimal image acquisition time for [^{18}F]FAPI-42 was determined to be 1 hour p.i. by comparing the ratios of small/large lesions to aortic lumen at different time points, which is consistent with the optimal image acquisition time of [^{18}F]FAPI-74 reported previously [27]. Although the uptake of [^{18}F]FAPI-42 in the tumors was rapid and high, the low TBR (blood) at the early 10-min scan made it unfavorable to detect some small lesions. It may not be necessary to postpone the [^{18}F]FAPI-42 scan to 2 hours because it did not show more tumor detection. It was observed that the radioactivity in the pancreas was obviously reduced in three patients after 2 hours, which may be useful for detection of pancreatic carcinoma. A similar phenomenon was reported such that [^{68}Ga]Ga-FAPI-04 detected pancreatic carcinoma using a 3-hour delay scan to reduce the physiologic radioactivity in the pancreas [31].

The biodistribution of [^{18}F]FAPI-42 in normal organs and tumor lesions was head-to-head compared with [^{68}Ga]Ga-FAPI-04 in the same twelve patients. The SUVmax analysis of the biodistribution of [^{68}Ga]Ga-FAPI-04 in our cohort was comparable with previously described data for [^{68}Ga]Ga-FAPI-04 [12, 30]. Comparison of the biodistribution of [^{18}F]FAPI-42 and [^{68}Ga]Ga-FAPI-04 in normal organs showed somewhat higher tracer uptake for [^{18}F]FAPI-42; however, this did not influence diagnostic accuracy (Fig. 4). This result might be due to the different lipophilicity of the NOTA-chelator and DOTA-chelator groups. Compared to [^{68}Ga]Ga-FAPI-04, [^{18}F]FAPI-42 showed a higher uptake in the parotid gland, submandibular gland, thyroid, myocardium, gallbladder, biliary tract, and pancreas, which might be caused by the different lipophilicity of the NOTA-chelator and DOTA-chelator groups. This shortcoming might influence the detection of lesions in these regions, especially for pancreatic, gallbladder and biliary tract tumors. [^{18}F]FAPI-42 accumulation in bone was low on PET/CT image in all patients, which indicated that no defluorination occurred *in vivo.* Of note, [^{18}F]FAPI-42 showed high bone uptake in preclinical mice models, as reported in our previous work and in the literature [20].

In the present study, we selected various tumors for [^{18}F]FAPI-42 scanning, including [^{18}F]FDG avid tumors, such as lung cancer, colorectal cancer and sarcoma, and some tumors prone to be [^{18}F]FDG non-avid, such as gastric cancer and hepatocellular cancer [32]. Our data indicated that all lesions were positive on [^{18}F]FAPI-42 scan, which implied that [^{18}F]FAPI-42 may play a supplementary role to [^{18}F]FDG, similar to recently reported of [^{68}Ga]Ga-FAPI-04 [20]. When compared with [^{68}Ga]Ga-FAPI-04, our results showed that [^{18}F]FAPI-42 had high uptake comparable to that of [^{68}Ga]Ga-FAPI-04 in the primary tumors, suspected lymph node metastases, pleural metastases and peritoneal metastases. The visual analysis also showed no significant differences between both tracers in the above lesions. Furthermore, [^{18}F]FAPI-42 showed superior detection ability compared to [^{68}Ga]Ga-FAPI-04 in liver and bone lesions based on the patient-based or lesion-based comparison, which was due to higher uptake and TBR in liver and bone tumors for [^{18}F]FAPI-42.

There are some limitations of the present study. Firstly, the dynamic scan was performed at early 20-min, but not 60-min, which could not provide more information concerning dynamic biodistribution of [^{18}F]FAPI-42 *in vivo*. In addition, our study is limited by the small sample size of the enrolled patients and limited tumor types. Further research is needed to investigate the real clinical value of [^{18}F]FAPI-42 in the diagnosing and staging of various tumors.

Conclusion

The biodistribution of [^{18}F]FAPI-42 showed high TBRs with increased over time and 1 hour was a suitable time for image acquisition. [^{18}F]FAPI-42 and [^{68}Ga]Ga-FAPI-04 exhibited comparably high lesion detectability in patients with various cancers. [^{18}F]FAPI-42 with the favorable characteristics is an attractive alternative to [^{68}Ga]Ga-FAPI-04.

Declarations

Acknowledgements We'd like to thank all the patients who participated in this study. We also thank the staff at the Department of Nuclear Medicine for their contribution to this work.

Authors' contributions Conception and design, K. Hu, and G. Tang; acquiring data, S. Huang, Y. Tian, Q. Wang, C. Xiao, L. Wang, and Y. Han;analysing data, L. Wang, Y. Han, Y. Tian, K. Hu, and H. Wu; drafting the manuscript: K. Hu, L. Wang, and H. Wu;revising the manuscript, G. Tang and Y. Han; enhancing the manuscript intellectual content: H. Wu**;** All authors read and approved the final manuscript.

Funding This work was supported in part by the National Natural Science Foundation of China (91949121), Guangdong Basic and Applied Basic Research Foundation (2021A1515011099), Outstanding Youths Development Scheme of Nanfang Hospital, Southern Medical University (2017J010), and Nanfang Hospital Talent Introduction Foundation of Southern Medical University (123456).

Ethics approval All procedures involving human participants were carried out in accordance with the Ethics Committee of Nanfang Hospital (No. NFEC-2020-205) and registered at Chinese Clinical Trial Registry (ChiCTR2100045757).

Consent to participate Written informed consent was obtained from all participants included in the study.

Consent for publication Not applicable.

Conflict of interest All the authors declare no competing interests.

References

1. Bušek P, Mal R, Šedo A. Dipeptidyl peptidase IV activity and / or structure homologues (DASH) and their substrates in cancer. Int J Biochem Cell Biol. 2004;36:408–21.

2. Liu F, Qi L, Liu B, Liu J, Zhang H, Che DH, et al. Fibroblast activation protein overexpression and clinical implications in solid tumors: a meta-analysis. PLoS One. 2015;10:1–18.

3. Yang L, Ma L, Lai D. Over-expression of fibroblast activation protein alpha increases tumor growth in xenografts of ovarian cancer cells. Acta Biochim Biophys Sin. 2013;928–37.

4. Busek P, Mateu R, Zubal M, Kotackova L, Sedo A. Targeting fibroblast activation protein in cancer–prospects and caveats. Front Biosci. 2018;1933–68.

5. van der Geest T, Roeleveld DM, Walgreen B, Helsen MM, Nayak TK, Klein C, et al. Imaging fibroblast activation protein to monitor therapeutic effects of neutralizing interleukin-22 in collagen-induced arthritis. Rheumatol. 2018;57:737–47.

6. Brokopp CE, Schoenauer R, Richards P, Bauer S, Lohmann C, Emmert MY, et al. Fibroblast activation protein is induced by inflammation and degrades type i collagen in thin-cap fibroatheromata. Eur Heart J. 2011;32:2713–22.

7. Fan MH, Zhu Q, Li HH, Ra HJ, Majumdar S, Gulick DL, et al. Fibroblast activation protein (FAP) accelerates collagen degradation and clearance from lungs in mice. J Biol Chem. 2016;291:8070–89.

8. Lay AJ, Zhang HE, Mccaughan GW, Gorrell MD, Fap S, Fap C, et al. Fibroblast activation protein in liver fibrosis. Front Biosci. 2019;1–17.

9. Rettig WJ, Garin-Chesa P, Beresford HR, Oettgen HF, Melamed MR, Old LJ. Cell-surface glycoproteins of human sarcomas: differential expression in normal and malignant tissues and cultured cells. Proc Natl Acad Sci U S A. 1988;85:3110–4.

10. Lindner T, Loktev A, Altmann A, Giesel F, Kratochwil C, Debus J, et al. Development of quinoline-based theranostic ligands for the targeting of fibroblast activation protein. J Nucl Med. 2018;59:1415–22.

11. Chen H, Pang Y, Wu J, Zhao L, Hao B, Wu J, et al. Comparison of [^{68}Ga]Ga-DOTA-FAPI-04 and [^{18}F]FDG PET/CT for the diagnosis of primary and metastatic lesions in patients with various types of cancer. Eur J Nucl Med Mol Imaging. 2020. doi: 10.1007/s00259-020-04769-z.

12. Loktev A, Lindner T, Mier W, Debus J, Altmann A, Jäger D, et al. A tumor-imaging method targeting cancer-associated fibroblasts. J Nucl Med. 2018;59:1423–9.

13. Kuten J, Levine C, Shamni O, Pelles S, Wolf I, Lahat G, et al. Head-to-head comparison of [^{68}Ga]Ga-FAPI-04 and [^{18}F]FDG PET/CT in evaluating the extent of disease in gastric adenocarcinoma. Eur J Nucl Med Mol Imaging. 2021. doi: 10.1007/s00259-021-05494-x.

14. Shi X, Xing H, Yang X, Li F, Yao S, Zhang H, et al. Fibroblast imaging of hepatic carcinoma with ^{68}Ga-FAPI-04 PET/CT : a pilot study in patients with suspected hepatic nodules. Eur J Nucl Med Mol Imaging. 2021. 48(1):196-203.

15. Kesch C, Yirga L, Dendl K, Handke A, Darr C, Krafft U, et al. High fibroblast-activation-protein expression in castration-resistant prostate cancer supports the use of FAPI-molecular theranostics. Eur J Nucl Med Mol Imaging. 2021;1–5.

16. Windisch P, Röhrich M, Regnery S, Tonndorf-martini E, Held T, Lang K, et al. Fibroblast activation protein (FAP) specific PET for advanced target volume delineation in Glioblastoma. Radiother Oncol. 2020;150:159-163.

17. Kratochwil C, Flechsig P, Lindner T, Abderrahim L, Altmann A, Mier W, et al. ^{68}Ga-FAPI PET/CT: tracer uptake in 28 different kinds of cancer. J Nucl Med. 2019;60:801–5.

18. Wang H, Zhu W, Ren S, Kong Y, Huang Q, Zhao J. Ga-FAPI-04 versus ^{18}F-FDG PET/CT in the detection of hepatocellular carcinoma. Front Oncol. 2021;11:693640.

19. Miller PW, Long NJ, Vilar R, Gee AD. Synthesis of ^{11}C, ^{18}F, ^{15}O, and ^{13}N radiolabels for positron emission tomography. Angew Chemie-Int Ed. 2008;47:8998–9033.

20. Wang S, Zhou X, Xu X, Ding J, Liu S, Hou X, et al. Clinical translational evaluation of Al^{18}F-NOTA-FAPI for fibroblast activation protein-targeted tumour imaging. Eur J Nucl Med Mol Imaging. 2021. doi:10.1007/s00259-021-05470-5.

21. Jiang X, Wang X, Shen T, Yao Y, Chen M, Li Z, et al. FAPI-04 PET/CT Using [^{18}F]AlF labeling strategy: automatic synthesis, quality control, and in vivo assessment in patient. Front Oncol. 2021;11:1–9.

22. Huang Y, Li H, Ye S, Tang G, Liang Y, Hu K. Synthesis and preclinical evaluation of an Al^{18}F radiofluorinated bivalent PSMA ligand. Eur J Med Chem. 2021;221:113502.

23. Loktev A, Lindner T, Burger EM, Altmann A, Giesel F, Kratochwil C, et al. Development of fibroblast activation protein-targeted radiotracers with improved tumor retention. J Nucl Med. 2019;60:1421–9.

24. Tan H, Sui X, Yin H, Yu H, Gu Y, Chen S, et al. Total-body PET/CT using half-dose FDG and compared with conventional PET/CT using full-dose FDG in lung cancer. Eur J Nucl Med Mol Imaging. 2021;48:1966–75.

25. Spencer BA, Berg E, Schmall JP, Omidvari N, Leung EK, Abdelhafez YG, et al. Performance evaluation of the uEXPLORER total-body PET/CT scanner based on NEMA NU 2-2018 with additional tests to characterize PET scanners with a long axial field of view. J Nucl Med. 2021;62:861–70.

26. Altmann A, Haberkorn U, Siveke J. The latest developments in imaging of fibroblast activation protein. J Nucl Med. 2021;62:160–7.

27. Giesel FL, Adeberg S, Syed M, Lindner T, Jiménez-Franco LD, Mavriopoulou E, et al. FAPI-74 PET/CT using either ^{18}F-AlF or cold-kit ^{68}Ga labeling: biodistribution, radiation dosimetry, and tumor delineation in

lung cancer patients. J Nucl Med. 2021;62:201–7.

28. Meyer C, Dahlbom M, Lindner T, Vauclin S, Mona C, Slavik R, et al. Radiation dosimetry and biodistribution of ^{68}Ga-FAPI-46 PET imaging in cancer patients. J Nucl Med. 2020;61:1171–7.

29. Toms J, Kogler J, Maschauer S, Daniel C, Schmidkonz C, Kuwert T, et al. Targeting fibroblast activation protein: radiosynthesis and preclinical evaluation of an ^{18}F-labeled FAP inhibitor. J Nucl Med. 2020;61:1806–13.

30. Wang S, Zhou X, Xu X, Ding J, Liu T, Jiang J, et al. Dynamic PET/CT imaging of ^{68}Ga-FAPI-04 in chinese subjects. Front Oncol. 2021;11:1–11.

31. Rohrich M, Naumann P, Giesel FL, Choyke PL, Staudinger F, Wefers A, et al. Impact of ^{68}Ga-FAPI PET/CT imaging on the therapeutic management of primary and recurrent pancreatic ductal adenocarcinomas. J Nucl Med. 2021;62:779–86.

32. Mankoff DA, Eary JF, Link JM, Muzi M, Rajendran JG, Spence AM, et al. Tumor-specific positron emission tomography imaging in patients: [^{18}F]fluorodeoxyglucose and beyond. Clin Cancer Res. 2007;13:3460–9.

Tables

Table 1 Patientcharacteristics

Patient No.	Gender	Age	Primary tumor site	Treatment	Pathology	Stage
1	Male	53	Lung	Operation	Squamous cell carcinoma	T4N2M1c, □
2	Male	63	Colon	None	Adenocarcinoma	cTxNxM1c, □C
3	Female	66	Lung	None	Adenocarcinoma	T1N3M1, □
4	Female	50	Colon	None	Adenocarcinoma	cT4N2bM1b, □B
5	Female	53	Colon	Operation	Adenocarcinoma	cTxNxM1c, □C
6	Male	58	Liver	Interventional therapy	Hepatocellular carcinoma	BCLC B
7	Female	61	Liver	Interventional therapy	Hepatocellular carcinoma	BCLC A
8	Male	58	Esophagus	Chemotherapy	Squamous cell carcinoma	cT4N2M0, □C
9	Male	59	Lung	None	Adenocarcinoma	T2aN3M1c, □B
10	Female	69	Celiac	None	Neuroendocrine carcinoma	T4N1M0, □
11	Male	47	Rectum	Operation	Adenocarcinoma	T3bN2aM0, □B
12	Male	52	Stomach	Operation	Adenocarcinoma	pT1aN3M0
13	Female	23	Colon	None	Adenocarcinoma	T4N2M1, □
14	Female	51	Bladder	Operation	Clear cell carcinoma	T3aN0M0, □A
15	Male	53	Lung	None	Adenocarcinoma	T3NxM1a, □
16	Male	36	Cheek	Operation	Carcinosarcoma	T4aN1M1, □
17	Female	51	Lung	None	Adenocarcinoma	T4N3M1b, □
18	Male	65	Liver	None	Hepatocellular carcinoma	BCLC C
19	Male	74	Lung	None	Squamous cell carcinoma	T4N3M0, □B
20	Female	59	Liver	Interventional therapy	Hepatocellular carcinoma	BCLC A
21	Male	64	Liver	None	Cholangiocarcinoma	T2bN1M1, □
22	Female	41	Liver	None	Cholangiocarcinoma	cT4N1M1, □

Table 2 Visual analysis of tumors on [^{18}F]FAPI-42 and [^{68}Ga]Ga-FAPI-04 PET/CT images.

Tumors	n	Positive detection		Visual analysis		
		[^{18}F]FAPI-42	[^{68}Ga]Ga-FAPI-04	[^{18}F]FAPI-42 > [^{68}Ga]Ga-FAPI-04	[^{18}F]FAPI-42 < [^{68}Ga]Ga-FAPI-04	[^{18}F]FAPI-42 = [^{68}Ga]Ga-FAPI-04
Primary/Relapse lesions	7	7	7	0	0	7
LN metastases	50	50	50	0	0	50
Lung metastases	4	4	4	0	0	4
Pleural metastases	21	21	21	0	0	21
Liver metastases	22	22	22	7	0	15
Bone metastases	17	17	17	5	0	12
Peritoneal metastases	10*	10	10	0	0	10
Others&	13	13	13	0	0	13
Total	144	144	144	12	0	132

* Patient 5 had diffuse uptake of FAP tracers in the peritoneum. We arbitrarily set the number of lesions to 10.

& including ovarian, pericardial, and adrenal metastases.

Figures

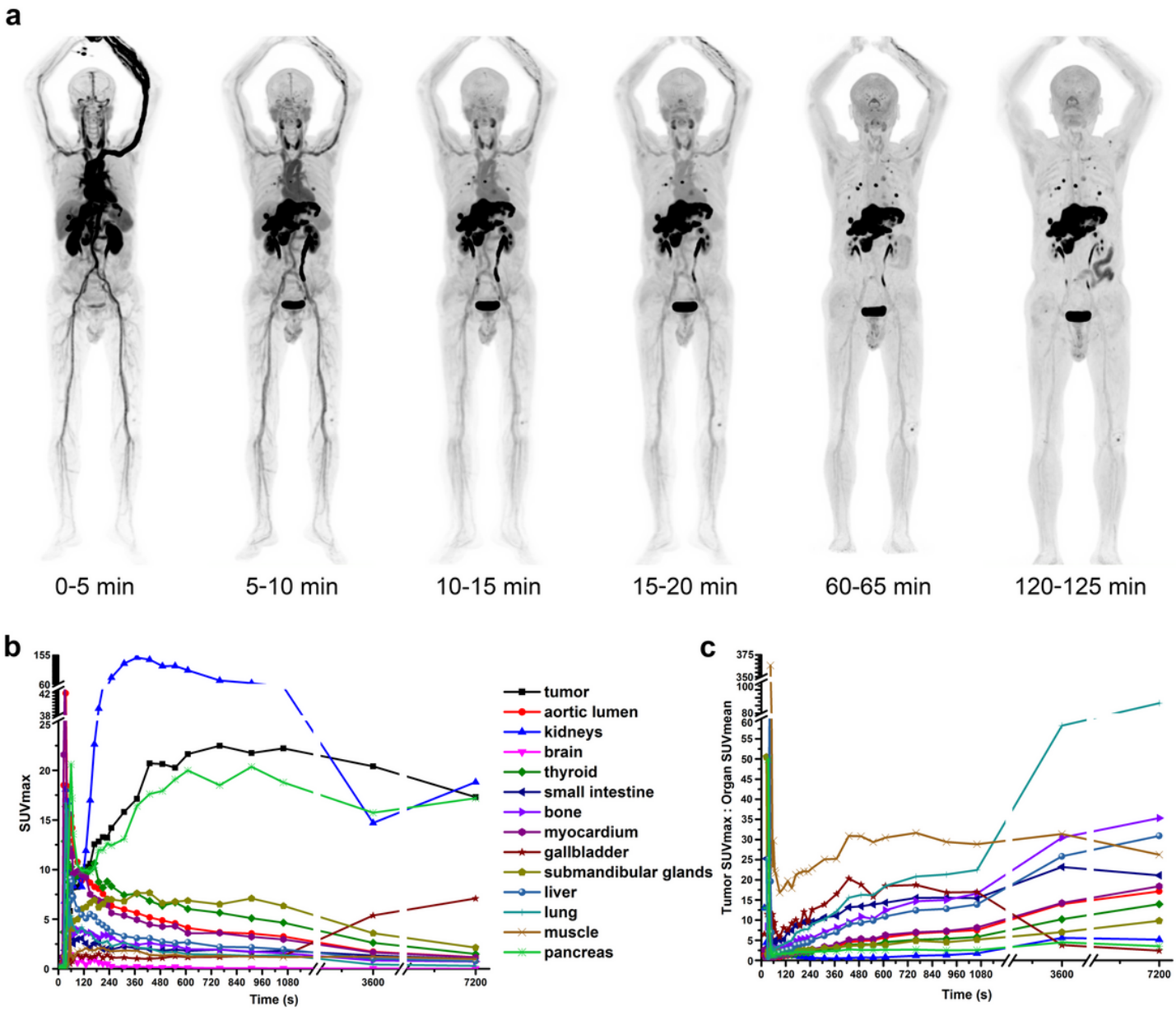

Figure 1

a Maximum intensity projection (MIP) of [18F]FAPI-42 at 5, 10, 15, 20, 65, and 120 min p.i. in patient 21 (female). b Time-activity-curves of [18F]FAPI-42 at different timepoints following tracer injection. c The ratios of tumor SUVmax/organ SUVmean at different timepoints following [18F]FAPI-42 injection. The ratio of tumor SUVmax/brain SUVmean was high and is excluded from the plot.

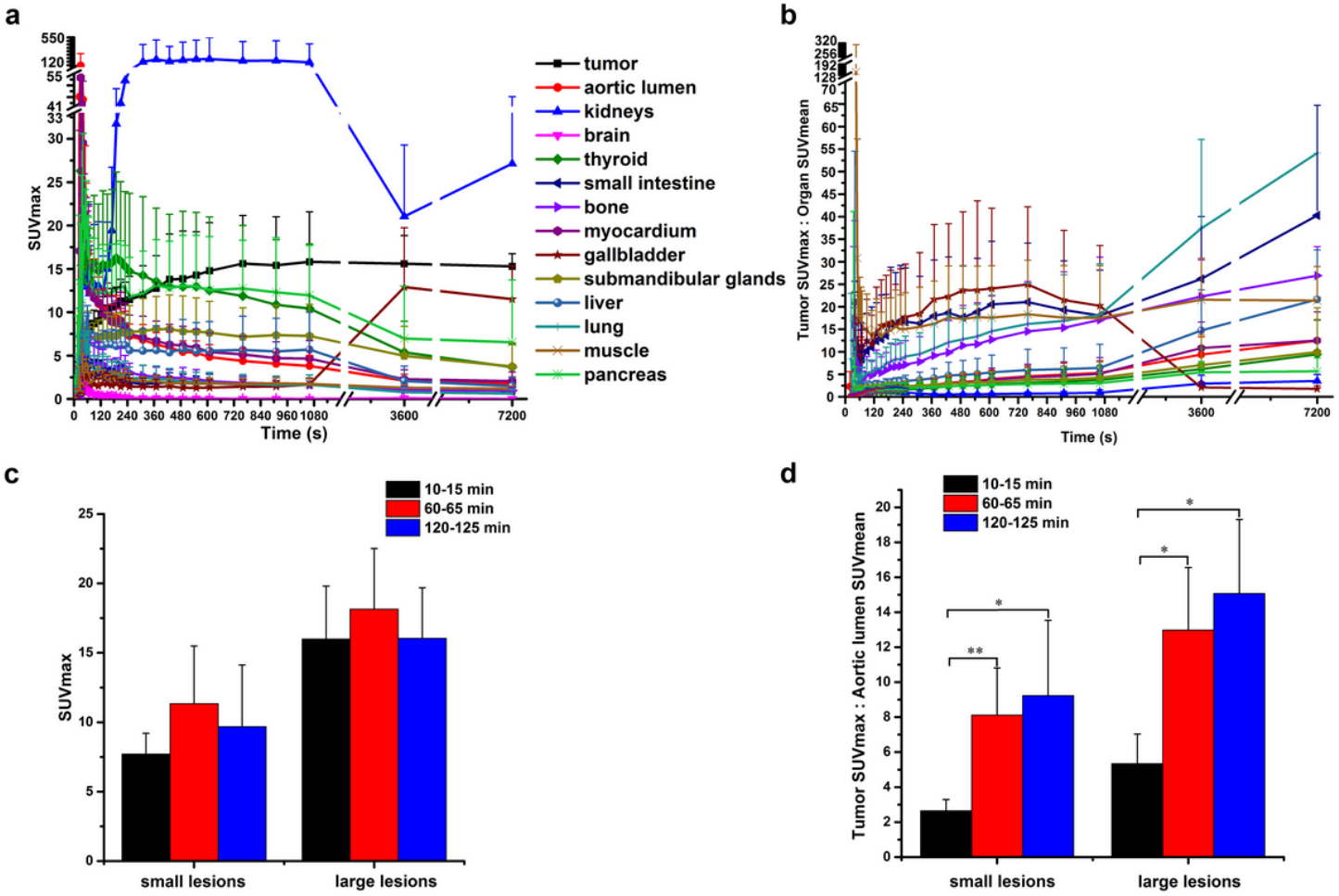

Figure 2

Pooled tumor and organ SUVmax (a) and ratios of tumor SUVmax/organ SUVmean at different timepoints following [18F]FAPI-42 injection (b). Pooled small and large tumor lesions SUVmax (c) and the ratios of tumor SUVmax/aortic lumen SUVmean (d) at 15, 65, and 120 min following [18F]FAPI-42 injection. Results are shown as the mean and standard deviation for 4 patients.

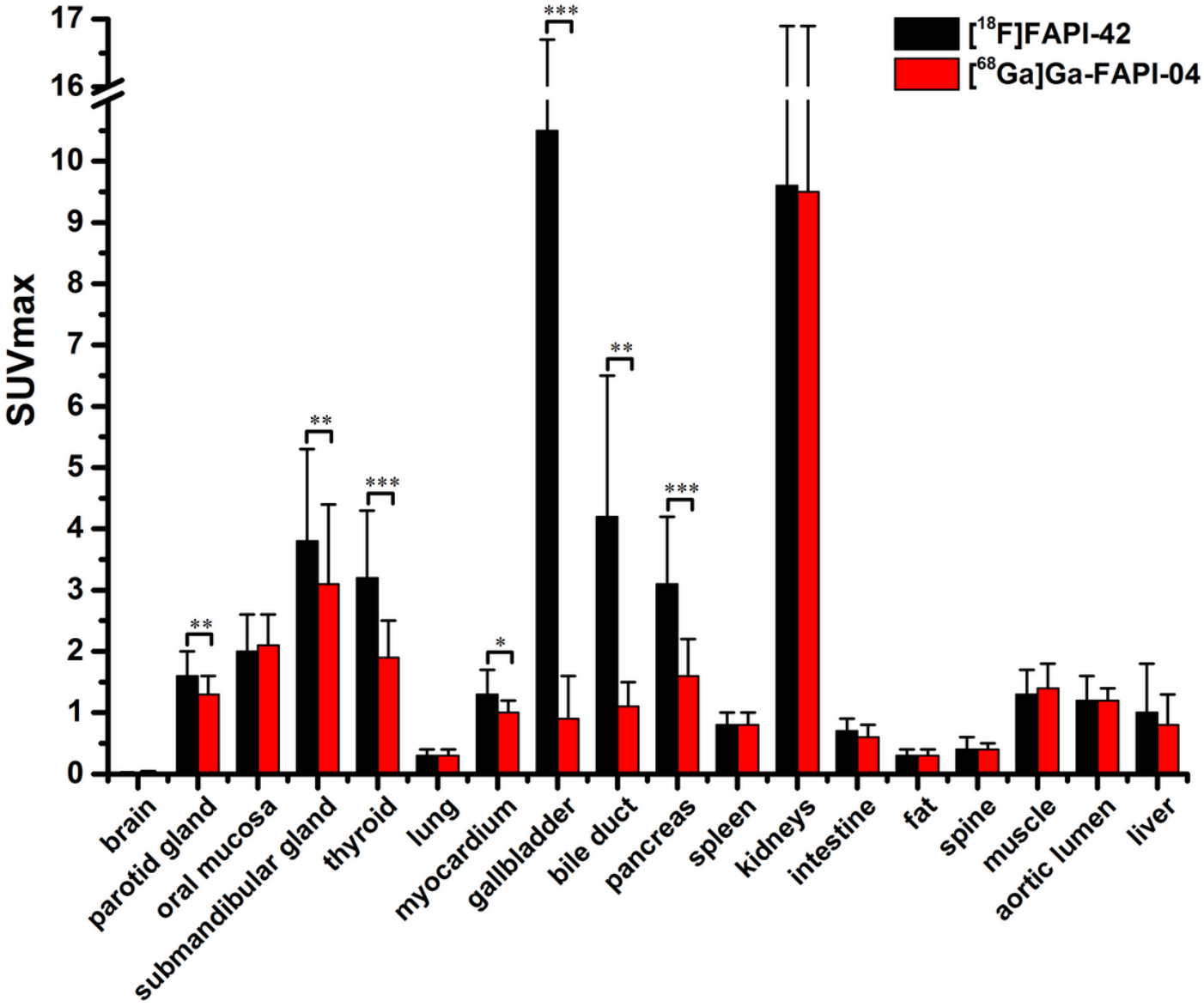

Figure 3

Biodistribution of SUVmax of [18F]FAPI-42 and [68Ga]Ga-FAPI-04 in normal organs at 1 h p.i. of the tracer. Results are shown as the mean and standard deviation for 12 patients.

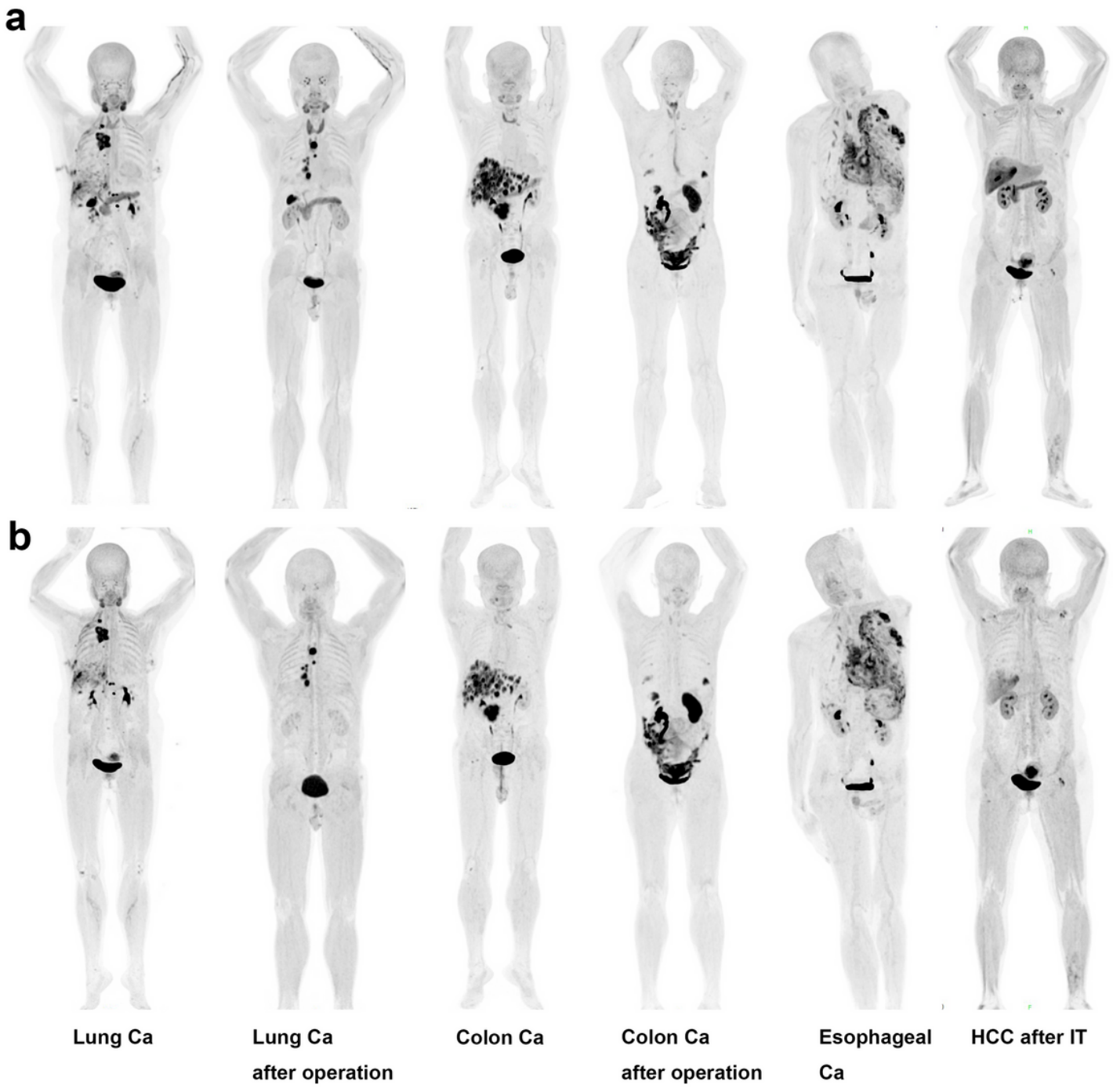

Figure 4

Maximum-intensity projections of [18F]FAPI-42 and [68Ga]Ga-FAPI-04 PET/CT in 6 representative patients (patients 3, 1, 2, 5, 8, and 7, from left to right) with different histologically proven tumor entities (sorted by tumor entity). Ca = cancer; HCC = hepatocellular carcinoma; IT = interventional therapy.

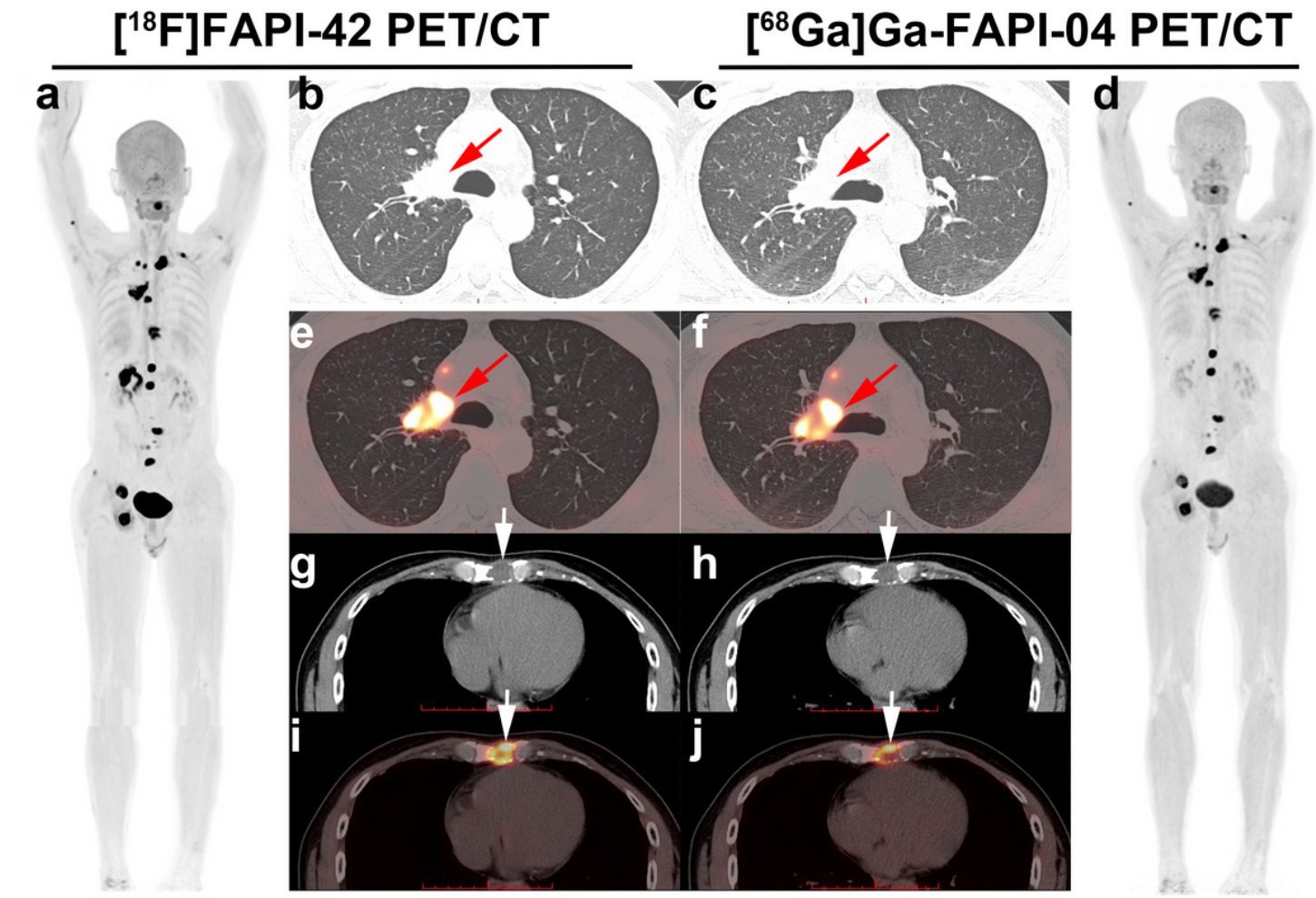

Figure 5

PET/CT images of [18F]FAPI-42 and [68Ga]Ga-FAPI-04 in patient 9 (male) with newly diagnosed lung adenocarcinoma. Both PET/CT detected the primary lung cancer (size 3.5 × 2.3 cm) in the upper lobe of the right lung with intense uptake of [18F]FAPI-42 (SUVmax 21.0; a and e) and [68Ga]Ga-FAPI-04 (SUVmax 17.3; d and f). Some bone metastases were more clearly visualized by [18F]FAPI-42 (a and i) compared with [68Ga]Ga-FAPI-04 PET/CT (d and j). a, d: MIP images; b, c and e, f: axial CT and fused PET/CT of the lung; g, h and i, j: axial CT and fused PET/CT of the mediastinum. The primary lung cancer is indicated by red arrows; bone metastasis is indicated by white arrows.

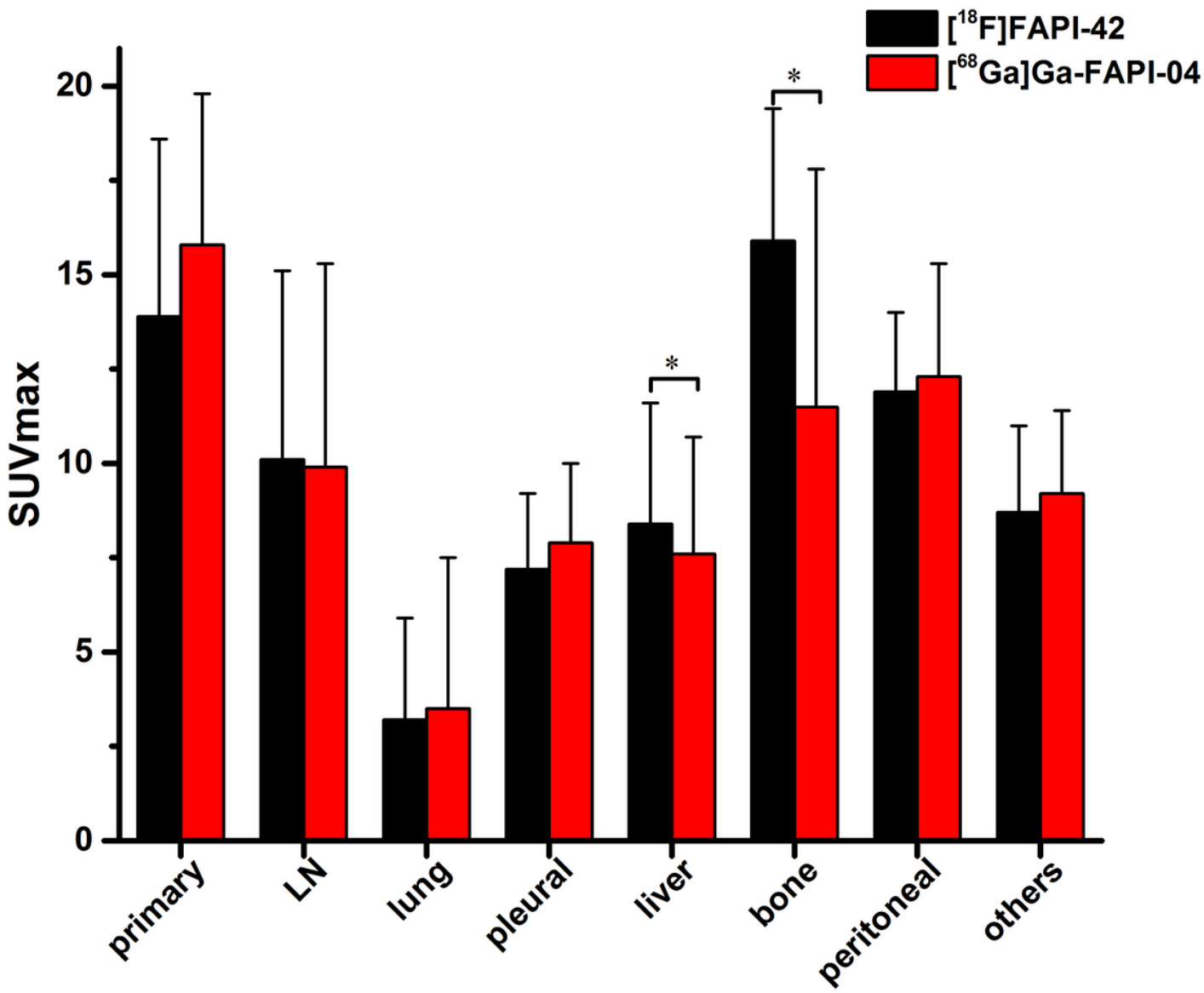

Figure 6

Tumor mean SUVmax of [18F]FAPI-42 and [68Ga]Ga-FAPI-04 at 1 hour p.i. (* P < 0.05).

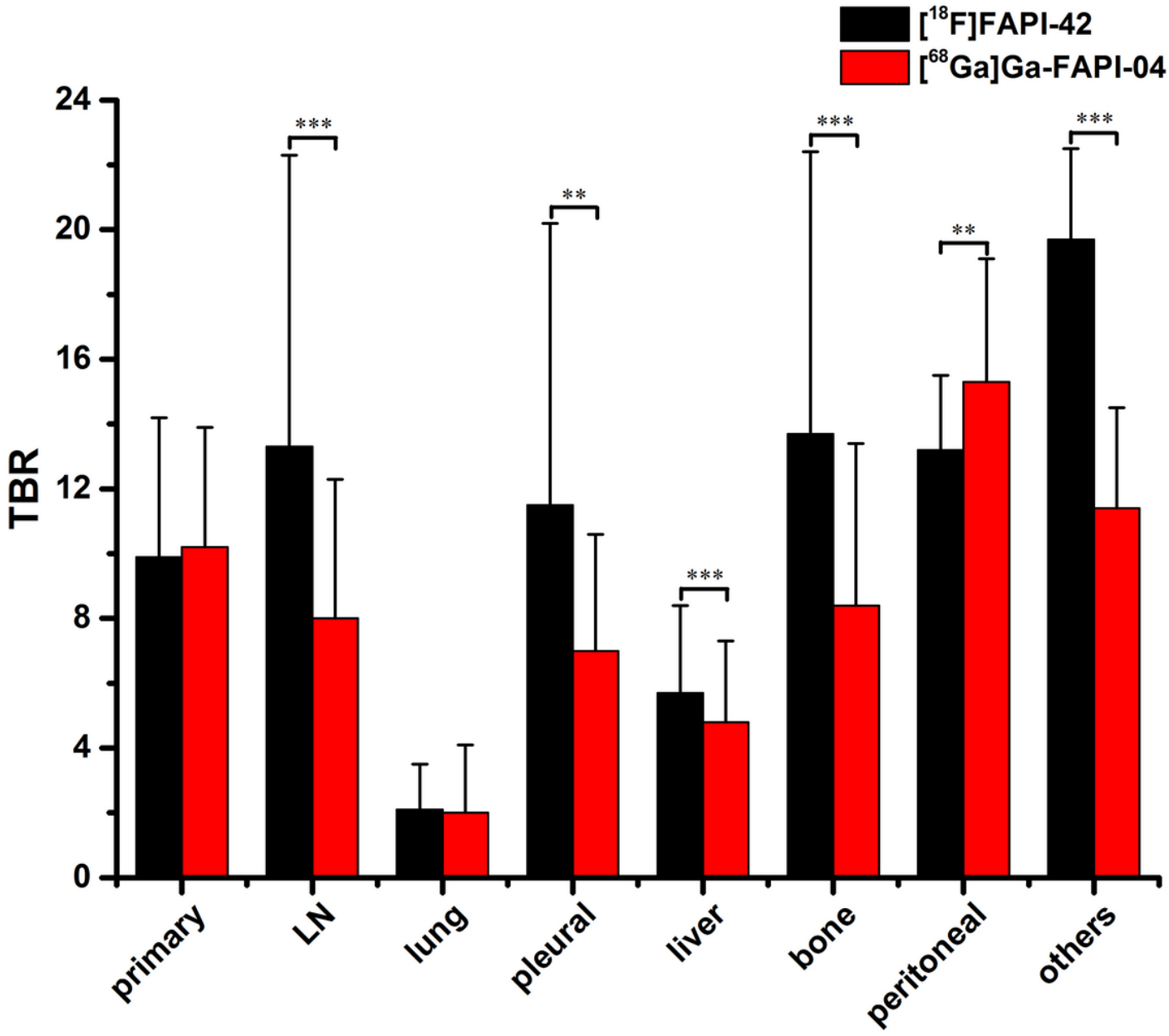

Figure 7

Tumor-to-background ratios of [18F]FAPI-42 and [68Ga]Ga-FAPI-04 at 1 hour p.i. (** P < 0.01, *** P < 0.001).

Supplementary Files

This is a list of supplementary files associated with this preprint. Click to download.

- SupplementalFigures.docx